Measurements of 3D slip velocities and plasma column lengths of a gliding arc discharge

Jiajian Zhu, Jinlong Gao, Andreas Ehn, Marcus Aldén, Zhongshan Li, Dmitry Moseev, Yukihiro Kusano, Mirko Salewski, Andreas Alpers, Peter Gritzmann, and Martin Schwenk

Citation: Applied Physics Letters **106**, 044101 (2015); doi: 10.1063/1.4906928
View online: http://dx.doi.org/10.1063/1.4906928
View Table of Contents: http://scitation.aip.org/content/aip/journal/apl/106/4?ver=pdfcov
Published by the AIP Publishing

Measurements of 3D slip velocities and plasma column lengths of a gliding arc discharge

Jiajian Zhu,[1,a)] Jinlong Gao,[1,a)] Andreas Ehn,[1,a)] Marcus Aldén,[1,a)] Zhongshan Li,[1,a),b)] Dmitry Moseev,[2,3,a)] Yukihiro Kusano,[4,a)] Mirko Salewski,[5,a)] Andreas Alpers,[6,b),c)] Peter Gritzmann,[6,c)] and Martin Schwenk[6,c)]

[1]*Division of Combustion Physics, Lund University, P.O. Box 118, S-221 00 Lund, Sweden*
[2]*Max-Planck-Institut für Plasmaphysik, D-85748 Garching bei München, Germany*
[3]*FOM Institute DIFFER, 3430 BE Nieuwegein, Netherlands*
[4]*Department of Wind Energy, Section for Composites and Materials Mechanics, Technical University of Denmark, Risø Campus, Frederiksborgvej 399, DK-4000 Roskilde, Denmark*
[5]*Department of Physics, Section for Plasma Physics and Fusion Energy, Technical University of Denmark, DK-2800 Kongens Lyngby, Denmark*
[6]*Zentrum Mathematik, Technische Universität München, D-85747 Garching bei München, Germany*

(Received 23 November 2014; accepted 18 January 2015; published online 28 January 2015)

A non-thermal gliding arc discharge was generated at atmospheric pressure in an air flow. The dynamics of the plasma column and tracer particles were recorded using two synchronized high-speed cameras. Whereas the data analysis for such systems has previously been performed in 2D (analyzing the single camera image), we provide here a 3D data analysis that includes 3D reconstructions of the plasma column and 3D particle tracking velocimetry based on discrete tomography methods. The 3D analysis, in particular, the determination of the 3D slip velocity between the plasma column and the gas flow, gives more realistic insight into the convection cooling process. Additionally, with the determination of the 3D slip velocity and the 3D length of the plasma column, we give more accurate estimates for the drag force, the electric field strength, the power per unit length, and the radius of the conducting zone of the plasma column. © *2015 AIP Publishing LLC*. [http://dx.doi.org/10.1063/1.4906928]

Much attention has recently been paid to generate and diagnose low-temperature plasmas at atmospheric pressure.[1–4] A gliding arc discharge is a typical low-temperature plasma source. The string-like plasma column of the gliding arc discharge is extended by a gas flow in three-dimensional (3D) space.[5,6] Such gliding arc discharges have been widely applied to pollution control,[7–11] surface treatment,[1,12] sterilization,[13] and combustion enhancement.[14] Extensive studies have been performed on the dynamics,[15–18] physical characteristics,[19–28] and chemical mechanisms[29–31] involved in gliding arc discharges. Phenomenological models[21,32–34] were developed to explain the discharge behavior based on accurate measurements of several important parameters, including the slip velocity $\vec{V}_S$ (it stands for the relative velocity between the plasma column $\vec{V}_C$ and the gas flow $\vec{V}_F$, and its magnitude is $|\vec{V}_S| = |\vec{V}_C - \vec{V}_F|$), and the length of the plasma column. The slip velocity determines not only the convection cooling efficiency[33] and the drag force[14,35] but also the electric field strength, the power per unit length, and the radius of the conducting zone of the plasma column.[33] The length of the plasma column is used for calculating the electric field strength.[6,32] Therefore, accurate measurements of the slip velocity and the length of the plasma column are essential to provide a better understanding of the gliding arc discharge.

In previous studies, measurements of the slip velocity and the length of the plasma column were performed in 2D, i.e., by analyzing a single 2D camera image.[21,33] The main limitation of this method is the lack of information about the 3D nature of the gliding arc discharge and the turbulent flow. In the present work, two high-speed cameras were synchronized to record images of the gliding arc in orthogonal imaging planes. Employing a dynamic discrete tomography approach,[36] we reconstructed the instantaneous 3D velocities of tracer particles illuminated by the plasma column. As the tracers particles are tiny ($\sim$3 μm), they follow the motion of the gas flow at the present moderated turbulent conditions. Since the particles are neutral and their concentration is kept low, their influence on the motion of the alternatively charged plasma columns can be negligible. Therefore, the tracers are suitable indicators for the local gas flow velocity. The plasma column and its velocity were also reconstructed in 3D. In particular, we determine here the 3D slip velocities and 3D plasma column lengths for a gliding arc discharge.

A schematic of the experimental setup is shown in Fig. 1. A gliding arc discharge at atmospheric pressure was generated between two diverging stainless steel electrodes using a 35 kHz AC power generator (9030E, SOFTAL Electronic GmbH, Germany). The peak voltage of the gliding arc discharge mostly varies from 3 to 12 kV.[15] The hollow electrodes with 3-mm outer diameter were internally water-cooled. Detailed descriptions of a similar gliding arc discharge system are available in previous works.[12,15–17] A total air flow of 17.5 Standard Liters per Minute (SLM) controlled by a mass flow controller (MFC) was divided into

[a)]Physics group
[b)]Authors to whom correspondence should be addressed. Electronic addresses: zhongshan.li@forbrf.lth.se and alpers@ma.tum.de
[c)]Mathematics group, in alphabetic order

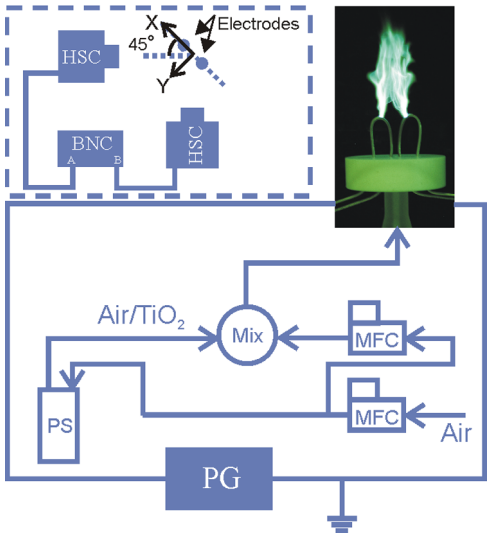

FIG. 1. Schematic of the experimental setup. HSC: high-speed camera; BNC: trigger pulse generator; MFC: mass flow controller; PS: particle seeder; and PG: power generator. The arrangement of the two cameras and the orientation of the electrodes are also illustrated.

two channels: one was controlled by an MFC at 16 SLM while the other ran through a particle seeder filled with TiO_2 particles. The air flows from the two channels were combined and sent into a 3-mm diameter hole to form a jet with exit velocity of 41 m/s; the air jet extended the plasma column in an upward direction.

The two high-speed cameras (Fastcam SA-X2 and Fastcam SA5, Photron) with 10-kHz frame rate and 99–μs exposure time were synchronized by a pulse generator (BNC 575) for simultaneously tracking the movement of the plasma column and the tracer particles, using two Nikon camera lenses (f = 50 mm and 100 mm). The arrangement of the two cameras and the gliding arc system is shown in Fig. 1, which also provides the coordinate system with the center of the jet nozzle representing the coordinate origin. Fig. 2 shows a typical

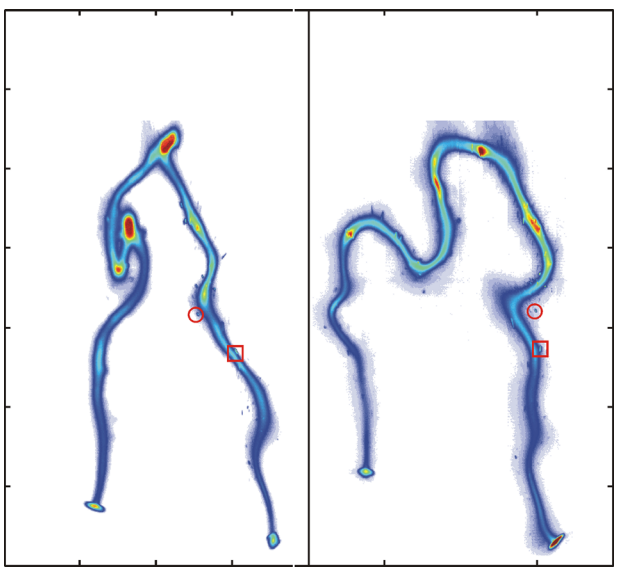

FIG. 2. An image pair of the gliding arc discharge simultaneously recorded by the two high-speed cameras. In this image, two typical seeding particles illuminated by the bright plasma column are highlighted by a red square and circle located on the right hand-side part of the plasma column.

camera image pair of the gliding arc. The tracer particles near the plasma column are illuminated by the plasma emission, and therefore can be simultaneously tracked by the two high-speed cameras as indicated in Fig. 2.[37]

For the 3D reconstruction of particle positions, we followed the recently introduced dynamic discrete tomography paradigm.[36] In this approach, the reconstruction task is formulated as a discrete optimization problem, which allows, in particular, for a detection of the time steps, for which the particle positions are uniquely determined by the data. The reported particle positions in this letter are mainly based on these time steps.

Prior to the reconstruction, we aligned the camera images and derived the viewing directions based on a set of calibration images. The camera pixel coordinates of the particles were obtained by iteratively/repeatedly applying a Gaussian blur filter followed by threshold filtering, which removed the plasma column data and resulted in single-pixel sized particles. For the reconstruction of the plasma column, we adapted an approach based on the deformation of the so-called snake model; for a similar approach, see Cai *et al.*[38]

For validation purposes, we compared the projections of the reconstructions with the experimental data. From this, we concluded that for the present data, an average uncertainty of 0.13 mm can be achieved.

Fig. 3 shows the reconstructed 3D plasma column together with 7 particles observed for 27 frames in a 4 ms time interval; the colors indicate the time evolution. Some plasma columns are not shown due to short-cutting events.[37]

The local gas flow velocities $\vec{V}_F$ are expressed by the 3D velocities of the seeding particles, provided by the 3D

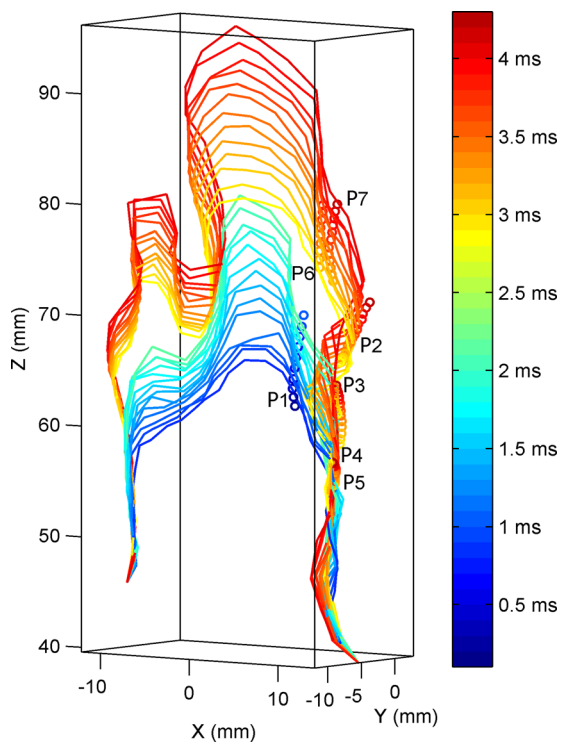

FIG. 3. 3D plasma column and particle reconstruction. Trajectories of seven seeding particles are marked (P1 to P7). The colors indicate the time evolution from 0 to 4 ms.

reconstruction of the particles. The determination of the 3D plasma column velocity $\vec{V_C}$ poses an additional challenge.[21] Here, the following strategy is adopted to determine the plasma column velocity:

(1) Each reconstructed plasma column is discretized by using 1500 equidistant nodes placed between the column endpoints.
(2) For each particle P_k in frame n, we determine the closest point Q_k on the discretized plasma column.
(3) For each Q_k, we determine the closest point R_k on the discretized plasma column in frame $n+1$.
(4) We determine the local plasma column velocity in frame n for particle P_k as $\vec{V_C} = (R_k – Q_k)/\Delta t$, where $R_k – Q_k$ denotes the distance between the two points and $\Delta t = 0.1$ ms denotes the time step between successive frames.

Figs. 4(a) and 4(b) show XZ and YZ components of the velocities of the seeding particles and plasma columns, indicating the horizontal (X-axis), lateral (Y-axis), and vertical (Z-axis) motion of the particles and the plasma columns. The thicker arrows represent the velocities of the particles while the thinner ones indicate the velocity of the plasma column with both the colors and the arrow length indicating the speed.

Fig. 4(c) shows the magnitude of the slip velocity, $\vec{V_S}$ ($|\vec{V_S}| = |\vec{V_C} - \vec{V_F}|$), between the plasma column and the gas flow. This magnitude was 2–8 m/s with an average of 4.5 m/s. The largest values were observed for Particles P6 and P7; the smallest value was observed for P5. It is generally believed that a larger magnitude of the slip velocity introduces a more efficient convection cooling.[33] In other words, here the convection cooling near P6 and P7 was more efficient than that near P5. This is reasonable since P6 and P7 were closer to the jet axis while P5 was located near the anchor point of the gliding arc. Previous results from 2D measurements showed that the speed difference was 1–10 m/s for a similar gliding arc discharge system (about 50 SLM flow rate and 2-mm diameter jet).[21,33] Note that in some measurement points, the plasma column speed was larger than the flow speed, which is not observed in previous results.[21,33]

Figs. 4(d) and 4(e) show the absolute difference between the slip speed obtained by 3D and 2D methods. For 3D method, all the motions in X, Y, Z directions are taken into consideration while 2D method just analyzes the motions in X, Z directions or Y, Z directions. The figures indicate that in some cases the slip speed can be underestimated by about 80% with the 2D method. This suggests that 3D visualization of the plasma column and the gas flow is essential to accurately determine the magnitude of the slip velocity.

The slip velocity enables the calculation of several parameters of the gliding arc discharge. The drag force F on the plasma column exerted by the turbulent flow is often modelled in the form[14,35]

$$\mathrm{F} = \frac{1}{2} C_D A \rho V_S^2, \tag{1}$$

where C_D is the drag coefficient, A the reference area, ρ the gas density, and V_S the magnitude of slip velocity. With the

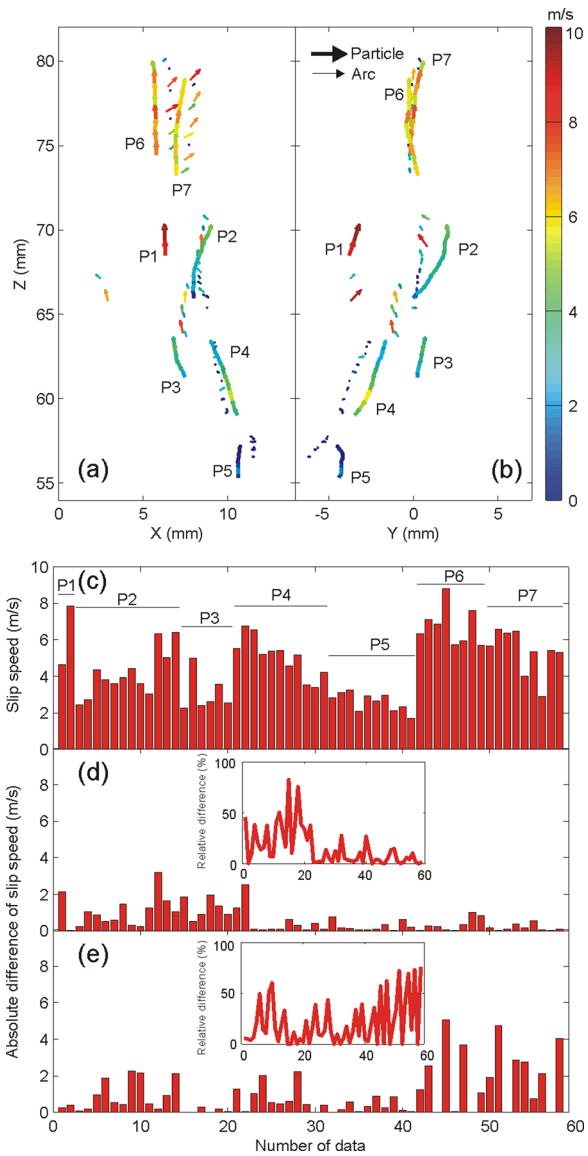

FIG. 4. Particle and plasma column velocity components in the (a) XZ and (b) YZ plane; (c) slip speed $|\vec{V_S}|$; (d) and (e) absolute difference between the slip speed obtained by the 3D and the 2D method (the 2D method is performed for the (d) XZ and (e) YZ components). Relative differences (given in %) are inserted as insets. Particles P1-P7 are labeled in (a), (b), and (c).

determination of drag force, the equilibrium velocity of the gliding arc discharge in hyper-gravity,[35] and the magnetic field strength of magnetically stabilized gliding arc discharge under steady state[14] can be calculated. This shows that knowledge of the 3D slip velocity is essential for predicting accurate parameters of the gliding arc discharge.

Furthermore, with the determination of the slip velocity, the electric field strength E, the power per unit length ω, and the radius of the plasma column conducting zone r can be calculated using the heat string model.[33] The model was developed for gliding arc discharges in atmospheric air. It was found from this model that E and ω are proportional to $V_S^{0.48}$ while r is proportional to $V_S^{-0.48}$. Here, V_S is the magnitude of the slip velocity. An underestimate of the slip speed by 80% introduced by 2D methods at the worst case can result in a 46% underestimate of E and ω, and an overestimate of r by a factor 2.

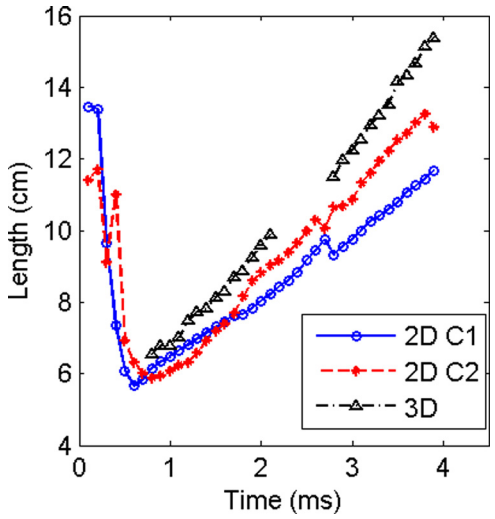

FIG. 5. Length of the plasma column based on the 3D reconstruction and, respectively, the 2D camera images.

Fig. 5 shows the length of the plasma column obtained from the 3D reconstruction and, respectively, from the 2D projections (measured on the two cameras C1 and C2, respectively). The plasma column estimated from the 3D reconstruction can be up to 25% longer than the corresponding 2D counterpart. This indicates that the traditional methods based on single 2D projections may overestimate the electrical field strength by about 25%. We remark that the short-cutting events are not included in the data processing, which cause the missing data points in Fig. 5.

In conclusion, 3D particle tracking velocimetry (PTV) and 3D reconstructions of the plasma column of a gliding arc discharge were performed, providing 3D measurements of the gas flow motion and the column movement. This 3D technique, in comparison to 2D methods, allowed a more accurate 3D determination of the slip velocity and the length of the plasma column. The magnitude of the 3D slip velocity is 2–8 m/s, while 2D methods may underestimate by up to 80%. The 3D length of the plasma column can likewise be 25% larger than the 2D length. Moreover, the 3D measurements of the slip velocity and the length of the plasma column yield more accurate estimates of the drag force, the electrical field strength, the power per unit length and the radius of the plasma column conducting zone, and provide a better understanding for the convection cooling.

The work at Lund was financially supported by the Swedish Energy Agency, the Knut and Alice Wallenberg Foundation, Swedish Research Council and the European Research Council. J. Zhu and J. Gao thank the Chinese Scholarship Council for financial support. A. Alpers, P. Gritzmann, and M. Schwenk were partly supported by DFG Grants AL 1431/1-1, GR 993/10-1, and GR 993/10-2. COST Action MP1207 is acknowledged for networking support.

[1]Z. B. Feng, N. Saeki, T. Kuroki, M. Tahara, and M. Okubo, Appl. Phys. Lett. **101**, 041602 (2012).
[2]X. Lu, Z. Xiong, F. Zhao, Y. Xian, Q. Xiong, W. Gong, C. Zou, Z. Jiang, and Y. Pan, Appl. Phys. Lett. **95**, 181501 (2009).
[3]S. Y. Moon, W. Choe, and B. K. Kang, Appl. Phys. Lett. **84**, 188 (2004).
[4]A. Shashurin, M. N. Shneider, A. Dogariu, R. B. Miles, and M. Keidar, Appl. Phys. Lett. **94**, 231504 (2009).
[5]A. Czernichowski, Pure Appl. Chem. **66**, 1301 (1994).
[6]A. Fridman, S. Nester, L. A. Kennedy, A. Saveliev, and O. Mutaf-Yardimci, Prog. Energy Combust. Sci. **25**, 211 (1999).
[7]J. H. Yan, C. M. Du, X. D. Li, X. D. Sun, M. J. Ni, K. F. Cen, and B. Cheron, Plasma Sources Sci. Technol. **14**, 637 (2005).
[8]X. Tu and J. C. Whitehead, Int. J. Hydrogen Energy **39**, 9658 (2014).
[9]V. Dalaine, J. M. Cormier, S. Pellerin, and P. Lefaucheux, J. Appl. Phys. **84**, 1215 (1998).
[10]V. Dalaine, J. M. Cormier, and P. Lefaucheux, J. Appl. Phys. **83**, 2435 (1998).
[11]Z. Bo, E. K. Wu, J. H. Yan, Y. Chi, and K. F. Cen, Rev. Sci. Instrum. **84**, 016105 (2013).
[12]Y. Kusano, B. F. Sorensen, T. L. Andersen, H. L. Toftegaard, F. Leipold, M. Salewski, Z. W. Sun, J. J. Zhu, Z. S. Li, and M. Aldén, J. Phys. D: Appl. Phys. **46**, 135203 (2013).
[13]C. M. Du, J. Wang, L. Zhang, H. X. Li, H. Liu, and Y. Xiong, New J. Phys. **14**, 013010 (2012).
[14]A. Fridman, A. Gutsol, S. Gangoli, Y. G. Ju, and T. Ombrellol, J. Propul. Power **24**, 1216 (2008).
[15]J. Zhu, J. Gao, Z. Li, A. Ehn, M. Aldén, A. Larsson, and Y. Kusano, Appl. Phys. Lett. **105**, 234102 (2014).
[16]J. Zhu, Z. Sun, Z. Li, A. Ehn, M. Aldén, M. Salewski, F. Leipold, and Y. Kusano, J. Phys. D: Appl. Phys. **47**, 295203 (2014).
[17]Z. W. Sun, J. J. Zhu, Z. S. Li, M. Aldén, F. Leipold, M. Salewski, and Y. Kusano, Opt. Express **21**, 6028 (2013).
[18]X. Tu, L. Yu, J. H. Yan, K. F. Cen, and B. G. Cheron, Phys. Plasmas **16**, 113506 (2009).
[19]T. L. Zhao, J. L. Liu, X. S. Li, J. B. Liu, Y. H. Song, Y. Xu, and A. M. Zhu, Phys. Plasmas **21**, 053507 (2014).
[20]C. Zhang, T. Shao, P. Yan, and Y. X. Zhou, Plasma Sources Sci. Technol. **23**, 035004 (2014).
[21]F. Richard, J. M. Cormier, S. Pellerin, and J. Chapelle, J. Appl. Phys. **79**, 2245 (1996).
[22]O. Mutaf-Yardimci, A. V. Saveliev, A. A. Fridman, and L. A. Kennedy, J. Appl. Phys. **87**, 1632 (2000).
[23]S. Y. Lu, X. M. Sun, X. D. Li, J. H. Yan, and C. M. Du, Phys. Plasmas **19**, 072122 (2012).
[24]I. V. Kuznetsova, N. Y. Kalashnikov, A. F. Gutsol, A. A. Fridman, and L. A. Kennedy, J. Appl. Phys. **92**, 4231 (2002).
[25]Y. D. Korolev, O. B. Frants, N. V. Landl, A. V. Bolotov, and V. O. Nekhoroshev, Plasma Sources Sci. Technol. **23**, 054016 (2014).
[26]Y. D. Korolev, O. B. Frants, V. G. Geyman, N. V. Landl, and V. S. Kasyanov, IEEE Trans. Plasma Sci. **39**, 3319 (2011).
[27]C. S. Kalra, Y. I. Cho, A. Gutsol, A. Fridman, and T. S. Rufael, Rev. Sci. Instrum. **76**, 025110 (2005).
[28]S. P. Gangoli, A. F. Gutsol, and A. A. Fridman, Plasma Sources Sci. Technol. **19**, 065004 (2010).
[29]R. Burlica, M. J. Kirkpatrick, and B. R. Locke, J. Electrost. **64**, 35 (2006).
[30]J. L. Brisset, D. Moussa, A. Doubla, E. Hnatiuc, B. Hnatiuc, G. K. Youbi, J. M. Herry, M. Naitali, and M. N. Bellon-Fontaine, Ind. Eng. Chem. Res. **47**, 5761 (2008).
[31]B. Benstaali, P. Boubert, B. G. Cheron, A. Addou, and J. L. Brisset, Plasma Chem. Plasma Process. **22**, 553 (2002).
[32]S. Pellerin, J. M. Cormier, F. Richard, K. Musiol, and J. Chapelle, J. Phys. D: Appl. Phys. **32**, 891 (1999).
[33]S. Pellerin, F. Richard, J. Chapelle, J. M. Cormier, and K. Musiol, J. Phys. D: Appl. Phys. **33**, 2407 (2000).
[34]Y. Kusano, M. Salewski, F. Leipold, J. Zhu, A. Ehn, Z. Li, and M. Aldén, Eur. Phys. J. D **68**, 319 (2014).
[35]J. Šperka, P. Souček, J. W. A. Loon, A. Dowson, C. Schwarz, J. Krause, G. Kroesen, and V. Kudrle, Eur. Phys. J. D **67**, 261 (2013).
[36]A. Alpers, P. Gritzmann, D. Moseev, and M. Salewski, Comput. Phys. Commun. **187**, 130 (2015).
[37]See supplementary material at http://dx.doi.org/10.1063/1.4906928 for showing the synchronized images of the plasma column and tracer particles (video 1.avi) and 3D details of the plasma column (video 2.avi).
[38]Y. Cai, Z. Su, Z. Li, R. Sun, X. Liu, and Y. Zhao, J. Comput. Appl. Math. **236**, 631 (2011).